Worldwide Geographical and Temporal Analysis of SARS-CoV-2 Haplotypes shows Differential Distribution Patterns

Santiago Justo Arévalo[1,2,*], Daniela Zapata Sifuentes[1,±], César Huallpa Robles[3,±], Gianfranco Landa Bianchi[1,±], Adriana Castillo Chávez[1,±], Romina Garavito-Salini Casas[1,±], Guillermo Uceda-Campos[2,4] Roberto Pineda Chavarría[1].

1.- Universidad Ricardo Palma, Facultad de Ciencias Biológicas, Lima – Perú.
2.- Universidade de Sao Paulo, Instituto de Química, Departamento de Bioquímica, São Paulo - Brasil
3.- Universidad Nacional Agraria La Molina, Facultad de Ciencias, Lima – Perú.
4.- Universidad Nacional Pedro Ruiz Gallo, Facultad de Ciencias Biológicas, Lambayeque - Perú
± These authors contributed equally to this work.
* Corresponding author: santiago.justo@urp.edu.pe

ABSTRACT:

Since the identification of SARS-CoV-2 in December 2019, a large number of SARS-CoV-2 genomes has been sequenced with unprecedented speed around the world and deposited in several databases. This marks a unique opportunity to study how a virus spreads and evolves in a worldwide context. However, currently there is not a useful haplotype classification system to help tracking the virus evolution. Here we identified eleven mutations with 10 % or more frequency in a data set of 7848 genomes. Using these mutations, we identified 6 SARS-CoV-2 haplotypes or OTUs (Operational Taxonomic Unit) that correlate well with a phylogenomic tree. After that, we analyzed the geographical and temporal distribution of these OTUs, as well as their correlation with patient status. Our geographical analysis showed different OTUs prevalence between continents and the temporal distribution analysis revealed an evolution-like pattern in SARS-CoV-2. Finally, we observed a homogenous distribution of OTUs in mild and severe patients and a great prevalence of OTU 2 in asymptomatic patients. However, genomes in the asymptomatic category, comes from isolates on three consecutive days in February (15 to 17), weakening this observation and highlighting the need to increase genomic analyzes in asymptomatic and severe patients. Our classification system is phylogenetically consistent and allows us to easily track geographic and temporal distribution of important mutations around the world. In the next months, it could be updated using similar steps that we used here.

INTRODUCTION:

COVID-19 was declared a pandemic by the World Health Organization on March 11th 2020[1], with around 10 million cases and 500 thousand of deaths around the world[2], quickly becoming the most important health concern in the world. Several efforts to produce vaccines, drugs and diagnostic tests to help in the fight against SARS-CoV-2 are being mounted in a large number of laboratories all around the world.

Since the publication on January 24th of the first complete genome sequence of SARS-CoV-2 from China[3], thousands of genomes have been sequenced in a great number of countries on all 5 continents and were made available in several databases. This marks a milestone in scientific history and gives us an unprecedented opportunity to study how a specific virus evolves in a worldwide context. As of June 09, 2020, the GISAID database[4] contained 27542 genomes with at least 29000 sequenced bases.

At the moment, some analysis has been performed to identify SARS-CoV-2 variants around the world, most of them on a particular group of genomes and/or at the beginning of the pandemic using limited datasets. In March, 2020 two major lineages were proposed based in position 8782

and 28144 using a data set of 103 genomes[5] which was followed by a particularly interesting proposal that identified the same major lineages (named A and B) and others sublineages[6]. Identification of SARS-CoV-2 variants aids in the understanding the evolution of the virus and may improve our efforts to control the disease.

We first used a "high-quality" data set of 7848 genomes from GISAID to perform a phylogenetic analysis and correlated the major branches with SARS-CoV-2 variants which can be classified into six haplotypes or OTUs (Operational Taxonomic Units) based on the distribution of the eleven most frequent mutations. After that, we classified 27542 genomes in these OTUs and analyzed the current geographical and temporal worldwide distribution of OTUs and attempt to correlate them with patient status information. We also discuss the possible implications of the most frequent mutations on protein structure and function.

RESULTS AND DISCUSSION:

Mutations frequency analysis

The GISAID database contains around 27542 genomes with at least 29000 sequenced bases (as of June 09th). To obtain high-quality data to perform the mutation frequency analysis we first filtered 19694 genomes that not meet our "high-quality" criteria (see material and methods).

With an alignment of our "high-quality" data set of 7848 genomes, we performed identity (respect to the reference sequence EPI_ISL_406801) and frequency analysis at each genomic position. We identified 11 positions with less than 0.9 identity (Fig. 1.A and S1.A) plus another other 15 positions with identities between 0.98 and 0.9 (Fig. S1.B) and many more positions with higher identities (Fig. S1.C).

The eleven most frequent mutations (less than 0.9 identity) are comprised of eight non-synonymous mutations, two synonymous mutations and one mutation in the 5'UTR region of SARS-CoV-2 genome (Fig. 1.A). All these mutations have been already identified in other studies[8,9,10], although with different frequencies.

OTUs identification

After the identity and frequency analysis, we estimated a maximum-likelihood tree using the whole-genome alignment of the 7848 genomes. Then, we associated the main branches of the whole-genome tree with an alignment of the 11 positions (241, 1059, 3037, 8782, 14408, 23403, 25563, 28144, 28881, 28882, 28883) and noted that combinations of those 11 positions represent 6 well-defined groups in the tree (Fig. 1.B). Using these combinations, we defined 6 haplotypes that allow us to classified more than 97 % of the analyzed genomes (Fig. 1.C). We named these haplotypes Operational Taxonomic Units (OTUs) and numbered them according to proximity to the root.

We were able to clearly track the mutations that originated each of these OTUs. OTU_1 is the ancestor haplotype with characteristic T8782 and C28144. Although a genome of this haplotype was not the first to be sequenced, these two positions (8782 and 28144) are also T and C, respectively, in the RaTG13 coronavirus[5]. This observation supports the idea that OTU_1 is the ancestor haplotype. OTU_2 differs from OTU_1 in position 8782 and 28144 (C and T, respectively in OTU_2). These two OTUs were already described in other analysis; in the begin of the pandemic, Tang et al (2020) shows linkage disequilibrium between those positions and named them as S (OTU_1) and L (OTU_2) lineages. Rambaut et al (2020) used these positions to discriminate between their proposed major lineages A (OTU_1) and B (OTU_2).

A SARS-CoV-2 isolated on February 20 was the first belonging to OTU_3 (Fig. S2) that shows simultaneously four mutations different to OTU_2 (C241T, C3037T, C14408T and A23403G). We can note in the phylogenetic tree that in the transition between the first clades and OTU_3 some unclassified tips were showed. These could be genomes containing some of these four mutations (C241T, C3037T, C14408T, A23403G) but not all, representing intermediate steps in the formation of this haplotype. OTU_3 is the first group containing the D614G mutation in the spike protein. Korber et al. 2020 analyzed the temporal and geographic distribution of this mutation separating SARS-CoV-2 populations into two groups, those with D614 and those with G614.

Almost at the same time (February 24), SARS-CoV-2 with three adjacent mutations (G28881A, G28882A and G28883C) (Fig. S2) in N protein was isolated. These three mutations characterize OTU_4. The maximum likelihood tree shows that OTU_5 comes from OTU_3. OTU_5 does not present mutations in N protein, instead, it presents a variation in Orf3a (G25563T). Finally, OTU_6 presents all the mutations of OTU_5 plus Nsp2 mutation (C1059T).

These 11 mutations have been separately described in other reports but, to our knowledge, they have not yet used been used together to classify SARS-CoV-2 variants during the pandemic. The fact that we were able to classify more than 97 % of the genomes in our “high-quality” data set (Fig. 1.C) shows that, at least to the present date, this classification system covers almost all the currently known genomic information around the world. Thus, at the moment this system can be of practical use to analyze the geographical and temporal distribution of haplotypes during these first five months of 2020.

It is highly likely is that during the next months, some of these OTUs will disappear and others will appear when new mutations in these “parental” OTUs become fixed in the population. Thus, methodologies to actively update this classification system on a real-time basis need to be proposed. We propose that the best strategy will be to continually monitor the appearance of new lineages by tracking mutations that exceed a fixed percentage of genomes in the database (to allow tracking of relevant medical mutations) and with the association of these mutations to a phylogenomic tree to confirm its phylogenetical relevance.

Unfortunately, the constancy of viral genomes sequencing efforts is highly variable around the world and over time, and it is likely that over time the amount of new genetic information of SARS-CoV-2 isolates will decrease. As we noted above, the number of sequenced genomes in April was much less than in March (Fig.S3). Thus, likely the cut-off used here to track a mutation (0.9 identity) could be changed in the next months.

Worldwide geographic distribution of OTUs

Using our OTUs classification, we analyzed the worldwide geographic distribution during the first five months of 2020. We began by plotting continental information in the unrooted tree of our “high-quality” data set (Fig. 2.A) and observed some interesting patterns. For instance, OTU_2 seems to be more prevalent in Asia, OTU_3 and 4 in Europe, and OTU_6 in North America (Fig. 2.A). However, this approach does not allow us to evaluate continents with less sequenced genomes (Fig. S2), such as South America, Oceania and Africa.

To better analyze which were the most prevalent OTUs in each continent, we analyzed all the complete genomes in GISAID database (27542 genomes). In this analysis, we randomly separate the genomes into 6 groups of 4590 genomes each and classified them into OTUs. Then, we independently analyzed each continent and sample, taking the percentages of OTUs in each

133 month and multiplying these percentages by the number of cases reported during that month.
134 Finally, these results were added to obtain a value for each OTU and the means of the six
135 samples were statistically compared (see material and methods for details).

136 This approach more clearly illustrates that OTU_6 was the most prevalent in North America,
137 followed by OTUs 1, 2, 3 and 5, the less prevalent was OTU_4 (Fig. 2.B). First genomes in North
138 America belonged to OTU_1 and 2, March and April showed similar OTUs counts with a tendency
139 to OTU_6 increment (Fig. S4). Finally, in May OTU_6 appear well established in North America
140 (Fig. S4). OTU_6 has 8 of the 11 high frequency genomic variations described (all except those
141 in N protein) (Fig. 5.C).

142 South America presents a more homogeneous distribution with OTU_4 in a statistically
143 significant greater proportion (Fig. 6.C). Apparently, this greater OTU_4 proportion in South
144 America was established in April (Fig. S4). Similarly, OTU_4 was most prevalent in Europe (Fig.
145 6.D). OTU_3 appears slightly less represented than OTU_4 but significatively than the other
146 OTUs (Fig. 6.D). At the haplotype level, OTU_4 present mutations in N protein that could
147 significantly increase the fitness of this group in comparison with OTU_3 that does not present
148 mutations in N (Fig. 1.A). We, therefore, believe that is important to more deeply study the
149 biological implications of these mutations.

150 Oceania presents OTU_2, 3 and 6 as the most prevalent (Fig. 6.F); in May, apparently, it shows
151 a homogeneous distribution of OTUs in the genomes sequenced (Fig. S4). The analysis of
152 Oceania is in part biased due the great percentage of genomes that we are not unambiguously
153 classified most genomes sequenced in Australia do not cover position 241 (in the 5` UTR region).

154 OTU_3 was the more prevalent in Africa, with all other OTUs represented in similar percentages
155 (Fig. 6.G).

156 In the case of Asia, we observed OTU_2 as the most prevalent during the months analyzed (Fig.
157 6.E). A detailed analysis of the sequenced genome counts by months in Asia (Fig. S4) shows that
158 this great OTU_2 representation is due to a high number of isolates during the first months of
159 the pandemic that correlated with the large number of cases in those months in Asia. Thus, the
160 first epicenter of the pandemic (Asia) was dominated by OTU_2; after that, as in other
161 continents, new haplotypes began to prevail.

162 **Worldwide temporal distribution of OTUs**

163 A rooted tree was estimated with our 7848 "high-quality" genomes data set and labeled by date
164 (Fig. 3.A). Here we can clearly follow the evolution beginning with OTU_1 and 2 at the base of
165 the tree (labeled with colors that correspond to the first months of the pandemic). The clade
166 where OTU_3 is the most prevalent has intermediate temporal distribution (late February up to
167 late April) and OTU_4, 5 and 6 have a more recent distribution pattern with representatives
168 isolated up to May.

169 To gain more insight into these patterns, we estimated the most prevalent OTUs during each
170 month of the pandemic following similar steps that those done for continents (see material and
171 methods). In this analysis, we did not consider December that present genomes just belonging
172 to OTU_2 (Fig.S4), or January that has representatives from OTU_1 and OTU_2 mainly from Asia
173 (Fig.S4 and Fig.S5).

174 Analysis using the data of February from North America, Europe and Asia showed that OTU_1
175 and 2 continue as the most prevalent in the world but with presence of OTU_3, 4, 5 and 6 (Fig.

176 3.B). Analysis by continents showed that during this month Asia and North America still had
177 higher proportions of OTU_1 and 2, but in Europe a more homogeneous distribution of OTUs 2-
178 6 was observed (Fig. S4).

179 In March, when the epicenter of pandemic move to Europe and North America, but cases were
180 still appearing in Asia, OTU_2, 3, 4 and 6 appear as the most prevalent (Fig. 3.C). Interestingly
181 OTU_5 remained in relatively low proportions (Fig. 3.C). Apparently, this month contain the
182 more homogenous OTUs distribution in a worldwide context, but with some OTUs more
183 prevalent in each continent (Fig. S4).

184 During April, OTU_1 continued its downward while OTU_5 increased its presence (Fig. 3.D)
185 probably due its higher representation (compared to March) in several continents such as South
186 America, North America and Asia (Fig. S4). During this month we also witnessed the
187 establishment of OTU_4 in South America and Europe and OTU_6 in North America (Fig. S4).

188 The last month analyzed (May) shows OTU_1 and 2 as the less prevalent; OTU_3, 4 and 5 in
189 similar proportions and OTU_6 as the significantly most prevalent in the world (Fig. 6.E) probably
190 because of its dominance in North America (Fig. S4). In this month, also we observed a
191 preponderance of isolated genomes belonging to OTU_5 in Asia (Fig. S4).

192 **Analysis of OTUs and patient status relation**

193 We attempt to analyze the patient status information in the GISAID database for roughly two
194 thousand genomes. Unfortunately, GISAID categories in patient status is not well organized and
195 we had to reclassify its information into four categories, Not Informative, Asymptomatic, Mild
196 and Severe (Fig. S6.A).

197 Using this classification scheme, we found that 44.83 % falls in the Not Informative category, 48
198 % in the Mild category, and just 3.22 % and 3.95 % of the genomes with patient status
199 information could be classified as Asymptomatic and Severe, respectively (Fig. S6.B). We
200 analyzed the group distribution in the three informative categories (Asymptomatic, Mild and
201 Severe).

202 Isolates from patients with mild symptoms presented a relatively homogeneous distribution,
203 with percentages between 21.7 % and 7.8 % from all six OTUs. The severe category was also
204 relatively homogeneous with OTU_1 being the least prevalent (3.7 %). Conversely, 86.4 % (57 of
205 the 66) of the genomes classified as Asymptomatic belong to OTU_2 (Fig. 4.B).

206 However, we have to interpret these observations with extreme caution since all the
207 asymptomatic genomes that belong to OTU_2 were isolated in Asia in February (Fig. S7.A) during
208 a short period of three days (Fig. S7.B). Other genomes from the asymptomatic group belong to
209 other OTUs and were isolated in different months and different continents (Fig. S7.B). Thus, we
210 currently require more robust information to obtain a better-defined distribution of
211 asymptomatic cases.

212 **Description of the most frequent mutations**

213 C241T

214 The C241T mutation is present in the 5` UTR region. In coronaviruses 5`UTR region is important
215 for viral transcription[11] and packaging[12]. Computational analysis showed that this mutation
216 could create a TAR DNA-binding protein 43 (TDP43) binding site[13], TDP43 is a well-characterized
217 RNA-binding protein that recognize UG-rich nucleic acids[14] described to regulate splicing of pre-

218 mRNA, mRNA stability and turnover, mRNA trafficking and can also function as a transcriptional
219 repressor and protect mRNAs under conditions of stress[15]. Experimental studies are necessary
220 to confirm different binding constants of TDP43 for the two variants of 5`UTR and its *in vivo*
221 effects.

222 C1059T

223 Mutation C1059T lies on Nsp2. Nsp2 does not have a clearly defined function in SARS-CoV-2
224 since the deletion of Nsp2 from SARS-CoV has little effect on viral titers and so may be
225 dispensable for viral replication[16]. However, Nsp2 from SARS-CoV can interact with prohibitin 1
226 and 2 (PBH1 and PBH2)[17], two proteins involved in several cellular functions including cell cycle
227 progression[18], cell migration[19], cellular differentiation[20], apoptosis[21] and mitochondrial
228 biogenesis[22].

229 C3037T and T8782C

230 Mutations C3037T and T8782C are synonymous mutations in Nsp3 and Nsp4 respectively,
231 therefore, is more difficult to associate these changes to an evolutionary advantage for the virus.
232 These two mutations occurred in the third position of a codon, one possibility is that this changes
233 the frequency of codon usage in humans increasing expression or any other of the related effects
234 caused by synonymous codon change (some of them reviewed[23]).

235 C3037T causes a codon change from TTC to TTT. TTT is more frequently present in the genome
236 of SARS-CoV-2 and other related coronaviruses compared to TTC[24] but in humans the codon
237 usage of TTT and TTC are similar[23]. The reason why TTT is more frequent in SARS-CoV-2 is
238 unknown but seems that is a selection related to SARS-CoV-2 and not by the host.

239 For T8782C, the change in codon is from AGT to AGC and opposite to C3037T, the mutated codon
240 (AGC) is less frequent than AGT in the SARS-CoV-2 genome[24] but AGC is more frequent than AGT
241 in human genomes[23]. In this case, seems that the change is related to an adaptation to human
242 host.

243 C14408T

244 The C14408T mutation changes P323 to leucine in Nsp12, the RNA-dependent RNA polymerase
245 of SARS-CoV2 (Fig. 5.A and B). P323, along with P322 end helix 10 and generate a turn preceding
246 a beta-sheet (Fig. 5.C). Leucine at position 323 could form hydrophobic interactions with methyl
247 group of L324 and the aromatic ring of F396 creating a more stable variant of Nsp12 (Fig. 5.E).
248 Protein dynamics simulations showed an increase in stability of the Nsp12 P323L variant[25]. In
249 absence of P322, the mutation P323L would probably be disfavored due to flexibilization of the
250 turn in the end of helix 10. Experimental evidence is necessary to confirm these hypotheses and
251 to evaluate its impact on protein function.

252 A23403G

253 An interesting protein to track is spike protein (Fig. 6.A) due to its importance in SARS-CoV-2
254 infectivity. It has been suggested that the D614G change in the S1 domain that results from the
255 A23403G mutation generates a more infectious virus, less spike shedding, greater incorporation
256 in pseudovirions[26] and higher viral load[7].

257 How these effects occur at the structural level remains unclear, although some hypotheses have
258 been put forward: 1) We think that there is no evidence for hydrogen-bond between D614 and
259 T859 mentioned by Korber et al. 2020, distances between D614 and T859 are too long for an

260 hydrogen bond (Fig 6.B), 2) distances between Q613 and T859 (Fig. 6.C) could be reduced by
261 increased flexibility due to D614G substitution, forming a stabilizing hydrogen bond, 3) currently
262 available structures do not show salt-bridges between D614 and R646 as proposed by Zhang et
263 al. 2020 (Fig. 6.D).

264 G25563T

265 Orf3a (Fig. 7.A) is required for efficient *in vitro* and *in vivo* replication in SARS-CoV[27], has been
266 implicated in inflammasome activation[28], apoptosis[29], necrotic cell death[30] and has been
267 observed in Golgi membranes[31] where pH is slightly acidic[32]. Kern et al. 2020 showed that Orf3a
268 preferentially transports Ca^{+2} or K^{+} ions through a pore (Fig 7.B) of in which one constriction is
269 formed by the side chain of Q57 (Fig.7.C).

270 Mutation G25563T produce a Q57H variant of Orf3a (Fig. 7.C) that did not show significant
271 differences in expression, stability, conductance, selectivity or gating behavior[8]. We modelled
272 Q57H mutation and we did not observe differences in the radius of constriction (Fig. 7.C) formed
273 by aminoacid 57 but we observed slightly differences in the electrostatic surface due the
274 ionizability of histidine side chain (Fig. 7.D).

275 C28144T

276 Orf8 is not well described in the literature and we cannot extrapolate results from SARS-CoV
277 because most of SARS-CoV genomes present a 29-nucleotide deletion that divides Orf8 into
278 Orf8a and Orf8b[33]. Recently, it was showed that Orf8a can directly interact with MHC-1
279 molecules and reduce their surface expression[34]. Also, they showed that in Orf8-expressing cells
280 MHC-1 molecules are target for lysosomal degradation[34]. However, they observed the same
281 downregulating effect for S84 (C28144) and L84 (T28144) Orf8 variants[34].

282 G28881A, G28882A, G28883C

283 N protein is formed by two domains and three disordered regions. The central disordered region
284 named LKR was shown to interact directly with RNA[35] and other proteins[36], probably through
285 positive side chains; also, this region contains phosphorylation sites able to modulate the
286 oligomerization of N protein[37].

287 Mutation G28883C that introduces an arginine at position 204 contributes one more positive
288 charge to each N protein. Mutations G28881A and G28882A produce a change from arginine to
289 lysine, these two positive amino acids probably have low impact in the overall electrostatic
290 distribution of N protein. However, change from R to K in this position could change the
291 probability of phosphorylation in S202 or T205. Using the program NetPhoK[38], we observed
292 different phosphorylation potential in S202 and T205 between G28881-G28882-G28883 (RG)
293 and A28881-A28882-C28883 (KR) (Fig. S8)

294 **CONCLUDING REMARKS:**

295 Here, we present a complete geographical and temporal worldwide distribution of SARS-CoV-2
296 haplotypes during the first five months of the pandemic. We identified 11 high frequency
297 mutations. These important variations (asserted mainly by their frequencies) need to be tracked
298 during the pandemic.

299 Our proposed classification system, showed to be phylogenetically consistent, allows us to easily
300 monitor the spatial and temporal changes of these mutations in a worldwide context. This was

only possible due the unprecedented worldwide efforts in genome sequencing of SARS-CoV-2 and the public databases that rapidly share the information.

In the next months, this classification system will need to be updated, identification of new haplotypes could be performed by combining identification of new frequent mutations (probably using less percentage cut-off than here, for example 1 %) and phylogenetic analysis. This classification can be useful to track SARS-CoV-2 evolution and dissemination of medical important mutations.

Our geographical analysis results showed a differential distribution pattern of OTUs in each continent. This could be due by different adaptations process in each continent, by evolutive characteristics and/or by lockdown policies. Temporal analysis showed an expected pattern of virus adaptation.

Our weak conclusion related to the patient status information is due the poorly organized metadata publicly available. Thus, we highlight the importance of correct management and organization genomic metadata.

Finally, although more studies need to be performed to increase our knowledge of the biology of SARS-CoV-2, we were able to make hypotheses about the possible effects of the most frequent mutations identified. This will help in the development of new studies that will impact vaccine development, diagnostic tests creation, among others.

MATERIAL AND METHODS:

Mutation frequency analysis:

To perform the mutation frequency analysis we first downloaded genomes from GISAID database (as of June 9th 2020) with more than 29000 nt, less than 1 % Ns, less than 0.05 % unique aminoacid mutations (not seen in other sequences in database), no insertion/deletion unless verified by submitter and with host description human or environment (27542 genomes downloaded). After that, we filtered genomes with any ambiguity using a python script (19278 genomes filtered). This set of genomes (8264 genomes) was aligned using MAFFT with FFT-NS-2 strategy and default parameter settings[39]. Finally, we manually removed genomes without sequence information from nt 203 to nt 29674 respect to the reference genome (EPI_ISL_406801), with a substitution in the stop codon of ORF10, with frameshifts in one or more ORFs, with any insertion and with 1, 2, 4 or more than 9 deletions. A list of all the manually removed genomes can be found in supplementary table 1. The final 7848 genomes ("high-quality" genomes data set) from nt 203 to 29674 (respect to the reference sequence) were aligned using MAFFT with FFT-NS-2 strategy and default parameter settings[39]. This alignment was used to calculate identity percentages based in the reference sequence and nucleotide frequency in each nucleotide genome position.

Phylogenetic tree construction:

Using the last alignment described in the previous section we estimated a maximum likelihood tree with IQ-TREE 2[40] using the GTR+F+R2 model of nucleotide substitution[41,42,43], default heuristic search options, ultrafast bootstrapping with 1000 replicates[44] and the reference genome as the outgroup.

OTUs determination:

342 Alignment of the identified mutations with 10 % or more frequency in our 7848 genomes dataset
343 were associated with the whole-genome rooted tree using the MSA function from the ggtree
344 package[45,46] in R, and visually examined to identify the major haplotypes based in these
345 positions, designated as OTUs (Operational Taxonomic Units).

346 **Analysis of OTUs geographical distribution:**

347 To perform these analysis we align using MAFFT with FFT-N-2 strategy[39] the 27542 genomes
348 with more than 29000 nt, less than 1 % Ns, less than 0.05 % unique aminoacid mutations (not
349 seen in other sequences in database), no insertion/deletion unless verified by submitter and
350 with host description human or environment from GISAID (as of June 9th 2020). After that, we
351 randomly select genomes and grouped them in six samples with 4590 genomes each. Genomes
352 in each sample were divided in continents and each continent in months. For each continent we
353 used the months with 25 or more total genomes in that month in that continent. We calculated
354 the percent of each OTU in each month analyzed. Then, we multiplied each OTU percent by the
355 number of cases reported in the analyzed continent and month (number of cases by continent
356 were obtained from European Centre for Disease Prevention and Control:
357 https://www.ecdc.europa.eu/en/publications-data/download-todays-data-geographic-
358 distribution-covid-19-cases-worldwide) (To count the number of cases in each continent in each
359 month we just used the data of the countries with at least one genome in our set of 27542
360 genomes) An example of the process of this analysis is showed in figure S9. Finally, we added by
361 OTUs the contribution of each month and averaged the results of the six samples. Statistical
362 difference between OTUs were calculated using the package "ggpubr" in R with the non-
363 parametric Kruskal-Wallis test, and pairwise statistical differences were calculated using non-
364 parametric Wilcoxon test from the same R package. Also, we plot the continent information of
365 each genome used to estimate the maximum likelihood tree to generate a tree figure with this
366 information using ggtree package in R[45,46].

367 **Analysis of OTUs temporal distribution:**

368 The same samples from the previous step, were now divided by months and each month by
369 continents. For each month we used the continents with 25 or more total genomes in that
370 continent in that month. The percentages of OTUs were calculated in each continent analyzed.
371 After that, we multiplied each OTU percent by the number of cases reported in the analyzed
372 month and continent (cases were obtained in the same form that in the previous section).
373 Finally, we added by OTUs the contribution of each continent and averaged the results of the six
374 samples. Final values were plotted and analyzed statistically as described in the previous section.
375 Also, we plot the collection date information of each genome used to estimate the maximum
376 likelihood tree to generate a tree figure with this information using ggtree package in R[45,46].

377 **Analysis of patient status with OTUs:**

378 2091 genomes with patient status information was downloaded from GISAID database.
379 Genomes with ambiguities in any of the positions necessary to classify the genomes in OTUs
380 were filtered (supplementary table 2 contain this information). The 2049 genomes remained
381 were aligned using MAFFT with FFT-NS-2 strategy and default parameter settings[39]. Using this
382 alingment we estimated a maximum likelihood tree with IQ-TREE 2[40] using the GTR+F+R5 model
383 of nucleotide substitution[41,42,43], default heuristic search options, ultrafast bootstrapping with
384 1000 replicates[44]. Patient status information from GISAID was recategorized in four disease
385 levels: No Informative, Asymptomatic, Mild and Severe. A table showing the GISAID patient
386 status categorize comprising our categories can be found in supplementary table 3. We plot the

387 information of these categories to our maximum likelihood tree of these genomes using ggtree
388 package in R[45,46], and calculate the frequency of OTUs in each patient status category.

389 **DATA AVAILABILITY:**

390 The data that support the findings of this study are available on request from the corresponding
391 author upon reasonable request.

392 **REFERENCES:**

393 1. Cuccinotta D and Vanelli M. 2020. WHO declares COVID-19 a pandemic. Vol. 91, 157-
394 160. Acta Biomedica.
395 2. WHO. 2020. https://www.who.int/emergencies/diseases/novel-coronavirus-2019
396 Retrieved on 02 July 2020.
397 3. Zhu N, Zhang D, Wang W, Li X, Yang B, Song J, Zhao X, Huang B, Shi W, Lu R, Niu P, Zhan
398 F, Ma X, Wang D, Xu W, Wu G, Gao G, Tan W. 2020. A novel coronavirus from patients
399 with pneumonia in China, 2019. Vol. 382(8), 727-733. The New England Journal of
400 Medicine.
401 4. Shu Y and McCauley J. 2017. GISAID: Global initiative on sharing all influenza data – from
402 vision to reality. Vol. 22(13), 1-3. Euro Surveillance.
403 5. Tang X, Wi C, Li X, Song Y, Yao X, Wu X, Duan Y, Zhang H, Wang Y, Qian Z, Cui J, Lu J.
404 2020. On the origin and continuing evolution of SARS-CoV-2. Vol. 7, 1012-1023. National
405 Science Review.
406 6. Rambaut A, Holmes E, Hill V, O`Toole A, McCrone A, Ruis C, du Plessis L, Pybus O. 2020.
407 A dynamic nomenclature proposal for SARS-CoV-2 to assist genomic epidemiology.
408 bioRxiv preprint doi: https://doi.org/10.1101/2020.04.17.046086.
409 7. Korber B, Fischer W, Gnanakaran S, Yoon H, Theiler J, Abfalterer W, Hengartner N, Giorgi
410 E, Bhattacharya T, Foley B, Hastie K, Parker M, Partridge D, Evans C, Freeman T, de Silva
411 T, McDanal C, Perez L, Tang H, Moon-Walker A, Whelan S, LaBranche C, Saphire E,
412 Montefiori D. 2020. Tracking changes in SARS-CoV-2 Spike: evidence that D614G
413 increases infectivity of the COVID-19 virus. https://doi.org/10.1016/j.cell.2020.06.043.
414 Cell.
415 8. Kern D, Sorum B, Hoel C, Sridharan S, Remis J, Toso D, Brohawn S. 2020. Cryo-EM
416 structure of the SARS-CoV-2 3a ion channel in lipid nanodiscs. bioRxiv preprint doi:
417 https://doi.org/10.1101/2020.06.17.156554.
418 9. Pachetti M, Marini B, Benedetti F, Giudici F, Mauro E, Storici P, Masciovecchio C,
419 Angeletti S, Ciccozzi M, Gallo R, Zella D, Ippodrino R. 2020. Emerging SARS-CoV-2
420 mutation hot spots include a novel RNA-dependent-RNA polymerase variant. Vol.
421 18(179), 1-9. Journal of Translational Medicine.
422 10. Yin C. 2020. Genotyping coronavirus SARS-CoV-2: methods and implication. Genomics.
423 https://doi.org/10.1016/j.ygeno.2020.04.016
424 11. Madhugiri R, Fricke M, Marz M, Ziebuhr J. 2014. RNA structure analysis of
425 alphacoronavirus terminal genome regions. Vol. 194, 76-89. Virus Research.
426 12. Masters P. 2019. Coronavirus genomic RNA packaging. Vol. 537, 198-207. Virology.
427 13. Mukherjee M and Goswami S. 2020. Global cataloguing of variations in untranslated
428 regions of viral genome and prediction of key host RNA binding protein-microRNA
429 interactions modulating genome stability in SARS-CoV-2. bioRxiv preprint doi:
430 https://doi.org/10.1101/2020.06.09.134585

431 14. Kuo P, Chiang C, Wang Y, Doudeva L, Yuan H. 2014. The crystal structure of TDP-43
432 RRM1-DNA complex reveals the specific recognition for UG- and TG-rich nucleic acids.
433 Vol. 42(7), 4712-4722. Nucleic Acids Research.
434 15. Lee E, Lee V, Trojanowski J. 2011. Gains or losses: molecular mechanisms of TDP43-
435 mediated neurodegeneration. Vol. 13(1), 38-50. Nature Reviews Neuroscience.
436 16. Graham R, Sims A, Brockway S, Baric S, Denison M. 2005. The nsp2 replicase proteins of
437 murine hepatitis virus and severe acute respirator syndrome coronavirus are
438 dispensable for viral replication. Vol. 79(21), 13399-13411. Journal of Virology.
439 17. Cornillez-Ty C, Liao L, Yates J, Kuhn P, Buchmeier M. 2009. Severe acute respiratory
440 syndrome coronavirus nonstructural protein 2 interacts with a host protein complex
441 involved in mitochondrial biogenesis and intracellular signaling. Vol. 83(19), 10314-
442 10318. Journal of Virology.
443 18. Wang S, Nath N, Adlam M, Chellappan S. 1999. Prohibitin, a potential tumor suppressor,
444 interacts with RB and regulates E2F function. Vol. 18, 3501-3510. Oncogene.
445 19. Rajalingam K, Wunder C, Brinkmann V, Churin Y, Hekman M, Sievers C, Rapp U, Rudel T.
446 2005. Prohibitin is required for RAS-induced RAF-MEK-ERK activation and epithelial cell
447 migration. Vol. 7(8), 837-843. Nature Cell Biology.
448 20. Sun L, Liu L, Yang X, Wu Z. 2004. Akt binds prohibitin 2 and relieves its repression of
449 MyoD and muscle differentiation. Vol. 117(14), 3021-3029. Journal of Cell Science
450 21. Fusaro G, Dasgupta P, Rastogi S, Joshi B, Chellappan S. 2003. Prohibitin induces the
451 transcriptional activity of p53 and is exported from the nucleus upon apoptotic signaling.
452 Vol. 278(48), 47853-47861. The Journal of Biological Chemistry.
453 22. Merkwirth C and Langer T. 2008. Prohibitin function within mitochondria: essential roles
454 for cell proliferation and cristae morphogenesis. Vol. 1793, 27-32. Biochimica et
455 Biophysica Acta.
456 23. Mauro V and Chapel S. 2014. A critical analysis of codon optimization in human
457 therapeutics. Vol. 20(11), 604-613. Trends in Molecular Medicine.
458 24. Gu H, Chu D Peiris M, Poon L. 2020. Multivariate Analyses of Codon Usage of SARS-CoV-
459 2 and other betacoronaviruses. bioRxiv preprint doi:
460 https://doi.org/10.1101/2020.02.15.950568.
461 25. Chand G and Azad G. 2020. Identification of novel mutations in RNA-dependent RNA
462 ploymerases of SARS-CoV-2 and their implications. bioRxiv preprint doi:
463 https://doi.org/10.1101/2020.05.05.079939.
464 26. Zhang L, Jackson C, Mou H, Ojha A, Rangarajan E, Izard T, Farzan M, Choe H. 2020. The
465 D614G mutation in the SARS-CoV-2 spike protein reduces S1 shedding and increases
466 infectivity. bioRxiv preprint doi: https://doi.org/10.1101/2020.06.12.148726.
467 27. Castaño-Rodriguez C, Honrubia J, Gutierrez-Alvarez J, DeDiego M, Nieto-Torres J,
468 Jimenez-Guardeño J,, Regla-Nava J, Fernandez-Delgado R, Verdia-Báguena C, Queralt-
469 Martín M, Kochan G, Perlman S, Aguilella V, Sola I, Enjuanes L. 2018. Role of severe acute
470 respiratory syndrome coronavirus viroporins E, 3a, and 8a in replication and
471 pathogenesis. Vol. 9(3), 1-23. American Society for Microbiology.
472 28. Siu K, Yuen K, Castaño-Rodriguez C, Ye Z, Yeung M, Fung S, Yuan S, Chan C, Yuen K,
473 Enjuanes L, Jin D. 2019. Severe acute respiratory syndrome coronavirus ORF3a protein
474 activates the NLRP3 inflammasome by promoting TRAF3-dependent ubiquitination of
475 ASC. Vol. 33. 8865-8877. The FASEB Journal.
476 29. Chan C, Tsoi H, Chan W, Zhai S, Wong C, Yao X, Chan W, Tsui S, Chan H. 2009. The ion
477 channel activity of the SARS-coronavirus 3a protein is linked to its pro-apoptotic
478 function. Vol. 41, 2232-2239. The International Journal of Biochemistry and Cell Biology

30. Yue Y, Nabar N, Shi C, Kamenyeva O, Xiao X, Hwang I, Wang M, Kehrl J. 2018. SARS-Coronavirus open reading frame-3a drives multimodal necrotic cell death. Vol. 9, 1-15. Cell Death and Disease.
31. Padhan K, Tanwar C, Hussain A, Hui P, Lee M, Cheung C, Malik J, Jameel S. 2007. Severe acute respiratory syndrome coronavirus Orf3a protein interacts with caveolin. Vol. 88, 3067-3077. Journal of General Virology.
32. Griffiths G and Simons K. 1986. The trans Golgi network: sorting at the exit site of the golgi complex. Vol. 234, 438-443. Science.
33. Lau S, Fen Y, Cheng H, Luk H, Yang W, Li K, Zhang Y, Huang Y, Song Z, Chow W, Fan R, Ahmed S, Yeung H, Lam C, Cai J, Wong Chan J, Yuen K, Zhang H, Woo P. 2015. Severe acute respiratory syndrome (SARS) coronavirus ORF8 protein is acquired from SARS-related coronavirus from greater horseshoe bats through recombination. Vol. 89(20), 10532-10547. Journal of Virology.
34. Zhang Y, Zhang J, Chen Y, Luo B, Yuan Y, Huang F, Yang T, Yu F, Liu J, Liu B, Song Z, Chen J, Pan T, Zhang X, Li Y, Li R, Huang W, Xiao F, Zhang H. 2020. The Orf8 protein of SARS-CoV-2 mediates immune evasion through potently downregulating MHC-1. bioRxiv preprint doi: https://doi.org/10.1101/2020.05.24.111823.
35. Chang C, Hsu Y, Chang Y, Chao F, Wu M, Huang Y, Hu C, Huang T. 2009. Multiple nucleic acid binding sites and intrinsic disorder of severe acute respiratory syndrome coronavirus nucleocapsid protein implications for ribonucleocapsid protein packaging. Vol. 83(5), 2255-2264. Journal of Virology.
36. Luo H, Chen Q, Chen J, Chen K, Shen X, Jiang H. 2005. The nucleocapsid protein of SARS coronavirus has a high binding affinity to the human cellular heterogeneous nuclear ribonucleoprotein A1. Vol. 579, 2623-2628. FEBS letters.
37. Chang C, Chen C, Chiang M, Hsu Y, Huang T. 2013. Transient oligomerization of the SARS-CoV N protein – Implication for virus ribonucleoprotein packaging. Vol. 8(5), e65045. PlosONE.
38. Blom N, Sicheritz-Pontén T, Gupta R, Gammeltoft S, Brunak S. 2004. Prediction of post-translationalo glycosylation and phophorylation of proteins from the aminoacid sequence. Vol. 4, 1633-1649. Proteomics.
39. Katoh K, Misawa K, Kuma K, Miyata T. 2002. MAFFT: a novel method for rapid multiple sequence alignment based on fast Fourier transform. Vol. 30(14), 3059-3066. Nucleic Acids Research.
40. Minh B, Schmidt H, Chernomor O, Schrempf D, Woodhams M, von Haeseler A, Lanfear R. 2020. IQ-TREE 2: New models and efficient methods for phylogenetic inference in the genomic era. Vol. 37, 1530-1534. Molecular Biology and Evolution.
41. Tavaré S. 1986. Some mathematical questions in biology: DNA sequence analysis. Lectures on mathematics in the life sciences. Vol. 17, 57-86. American Mathematical society.
42. Soubrier J, Steel M, Lee M, Sarkissian C, Guindon S, Ho S, Cooper A. 2012. The influence of rate heterogeneity among sites on the time dependence of molecular rates. Vol. 29(11), 3345-3358. Molecular Biology and Evolution.
43. Yang Z. 1995. A space-time process model for the evolution of DNA sequences. Vol. 139, 993-1005. Genetics
44. Hoang D, Chernomor O, Haeseler A, Minh B, Vinh L. 2017. UFBoot2: Improving the ultrafast bootstrap approximation. Vol. 35(2), 518-522. Molecular Biology and Evolution.

45. Yu G. 2020. Using ggtree to visualize data on tree-like structures. Vol. 69, 1-18- Current Protocols in Bioinformatics.
46. Yu G, Smith D, Zhu H, Guan Y, Lam T. 2017. GGTREE: an R package for visualization and annotation of phylogenetic trees with their covariates and other associated data. Vol. 8, 28-36. Methods in Ecology and Evolution.

Author contributions:

S.J.A., D.Z.S., C.H.R., G.L.B., A.C.C. and R.G.C. conceived, initiated and coordinated the project. S.J.A. performed the phylogenetic analyses, geographical and temporal analyses. G.U.C. wrote python scripts used in data processing and analyses. S.J.A., D.Z.S., C.H.R., G.L.B., A.C.C., R.G.C., R.P.C. performed the structural analysis. Manuscript was written by S.J.A., D.Z.S., C.H.R., G.L.B. All authors discussed the methodologies, results, read and approved the manuscript.

Acknowledgements:

We thank Professor Shaker Chuck Farah (Institute of Chemistry – University of Sao Paulo) for English writing corrections and helpful comments. Also, we thank Professors Aline Maria da Silva (Institute of Chemistry – University of Sao Paulo), Joao Renato Rebello Pinho (Albert Einstein Hospital – Sao Paulo) and PhD(c). Deyvid Amgarten (Albert Einstein Hospital – Sao Paulo) for its helpful comments. To the Ricardo Palma University High-Performance Computational Cluster (URPHPC) managers Gustavo Adolfo Abarca Valdiviezo and Roxana Paola Mier Hermoza at the Ricardo Palma Informatic Department (OFICIC) for their contribution in programs and remote use configuration of URPHPC. To Gladys Arevalo Chong for her figure style suggestions.

Competing interests:

The authors declare no competing interests

A)

Position	OTU						Region	AA change	Identity*
	1	2	3	4	5	6			
241	C	C	T	T	T	T	5' UTR	----	0.276
1059	C	C	C	C	C	T	Nsp2	T85I	0.773
3037	C	C	T	T	T	T	Nsp3	Syn	0.281
8782	T	C	C	C	C	C	Nsp4	Syn	0.100
14408	C	C	T	T	T	T	Nsp12	P323L	0.278
23403	A	A	G	G	G	G	S	D614G	0.275
25563	G	G	G	G	T	T	Orf3a	Q57H	0.676
28144	C	T	T	T	T	T	Orf8	S84L	0.103
28881	G	G	G	A	G	G	N	R203K	0.813
28882	G	G	G	A	G	G	N	R203K	0.813
28883	G	G	G	C	G	G	N	G204R	0.813

B)

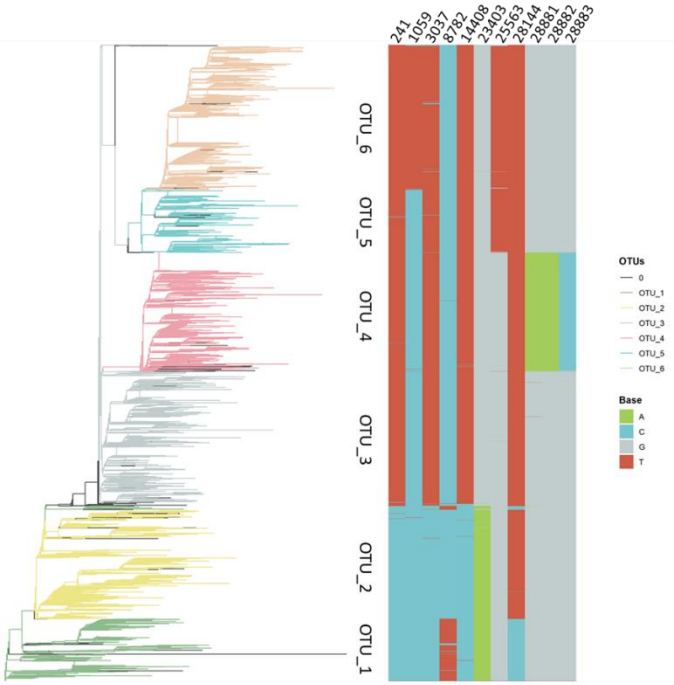

C)

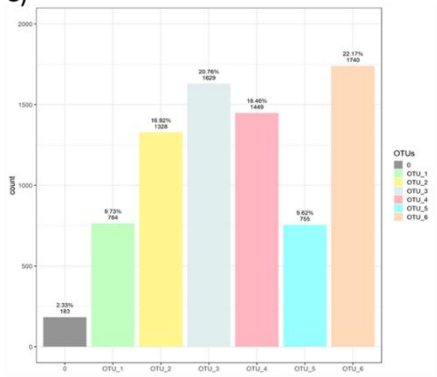

Figure 1. Six haplotypes based in eleven positions can classify more than 97 % of the genomes. A) Rooted tree of 7848 SARS-CoV-2 complete genomes associated to an alingment of eleven genomic positions (241, 1059, 3037, 8782, 14408, 23403, 25563, 28144, 28881, 28882, 28883) showing well correlation between haplotypes (OTUs) based in these eleven positions. Tips of the tree where colored based in the OTU. B) Bar diagram shows the OTUs distribution of the 7848 genomes (0 correspond to unclassified genomes). C) Table showing the haplotype of each OTU.

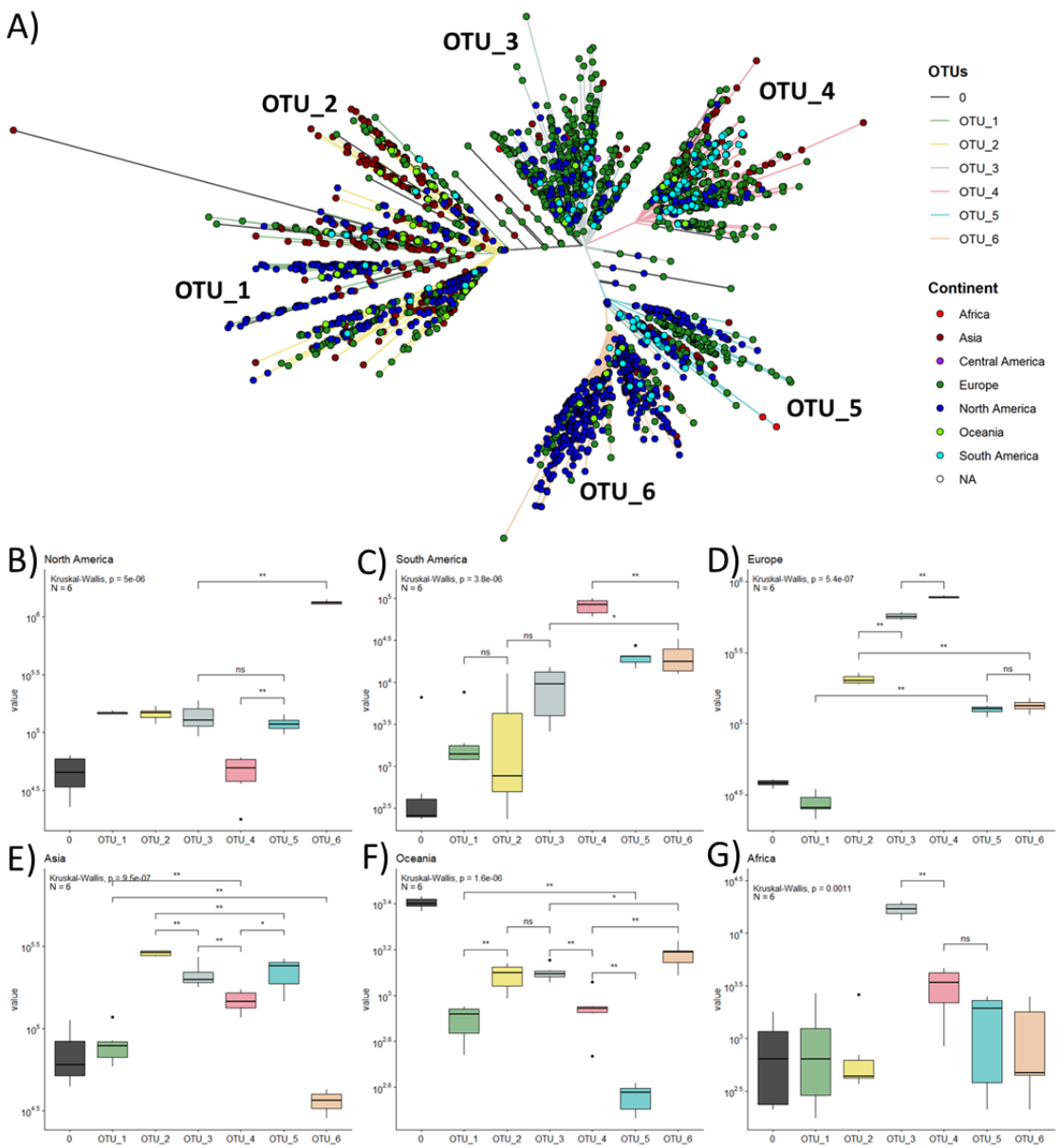

Figure 2. Differential distribution of genotypes showed by worldwide geographic analysis. A) Unrooted tree of the 7848 genomes, tips were colored according to OTUs and points in each tip were colored according to continent. B-G) Boxplots of OTUs distribution in each continent (B, North America; C, South America; D, Europe; E, Asia; F, Oceania; G, Africa).

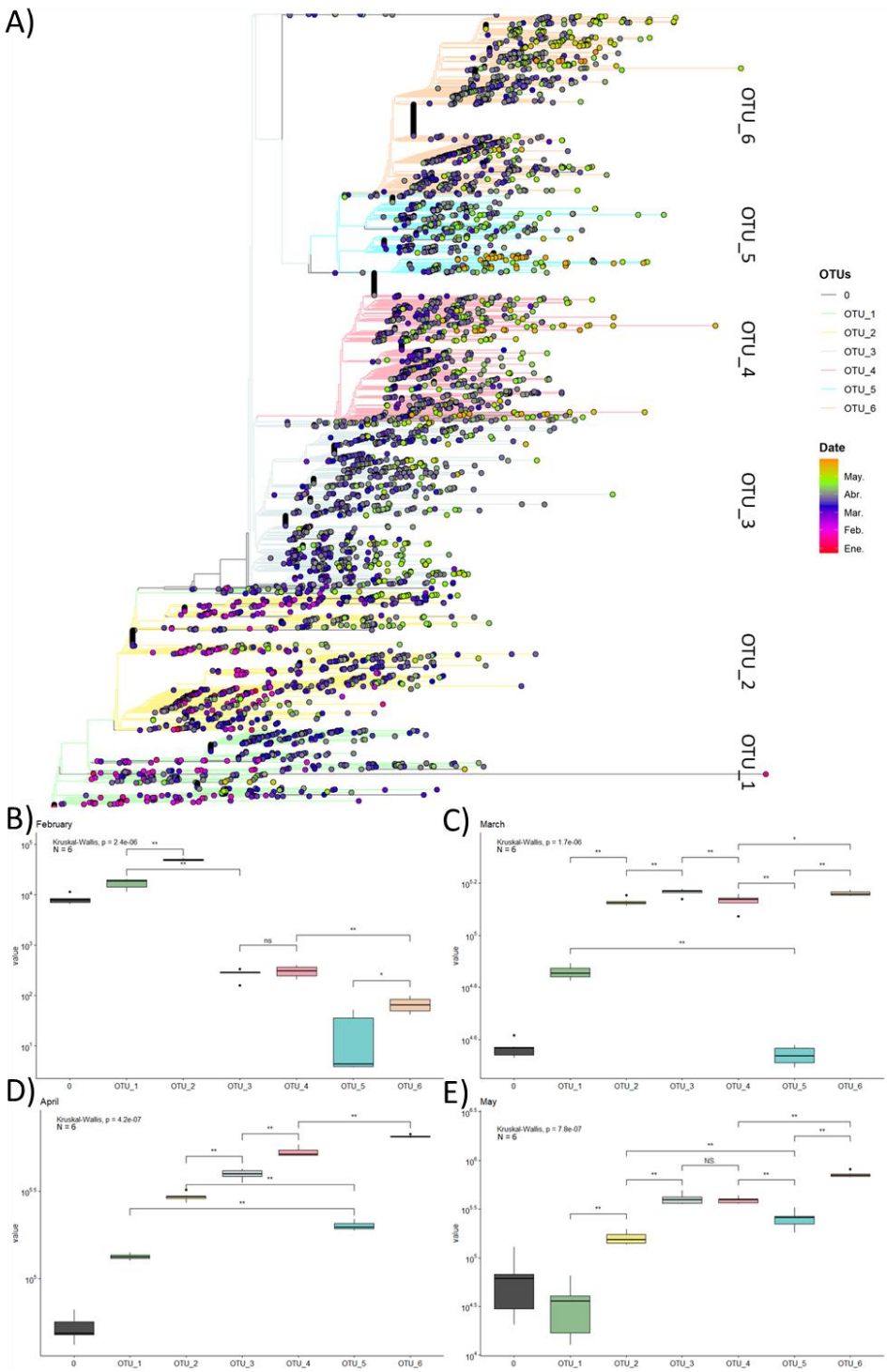

Figure 3. Evidence of evolution in SARS-CoV-2 showed by worldwide temporal distribution analysis. A) Rooted tree of the 7848 genomes showing temporal distribution. Tips were colored by OTUs and point in each tip were colored according to the isolation date of the genome. B-E) Boxplot of OTUs distribution in each month (B, February; C, March; D, April; E, May).

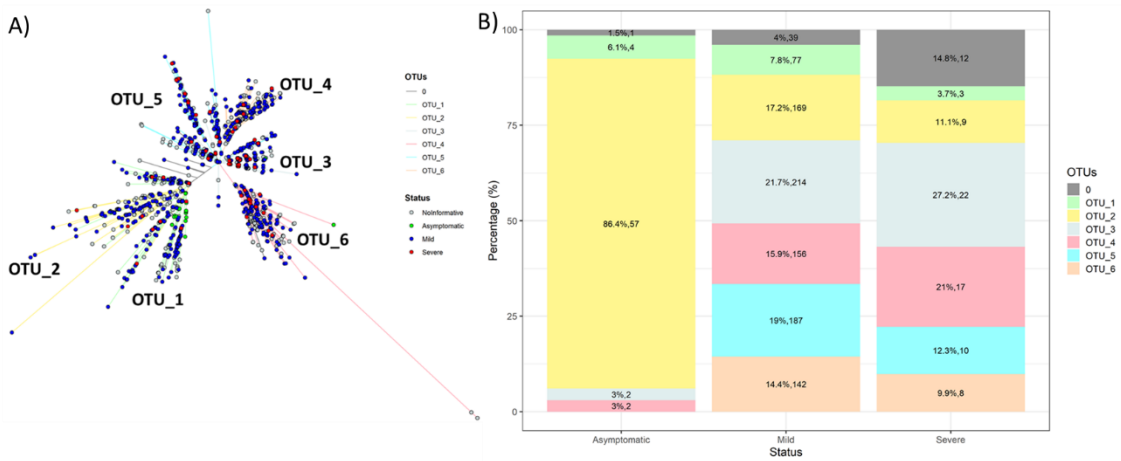

Figure 4. Scarce number of genomes with patient status avoid robust conclusions. A) Unrooted tree of 2050 genomes with patient status information in GISAID database. Tips were colored by OTUs and points in each tip were colored by Status. B) Percentages by OTUs by patient status categories.

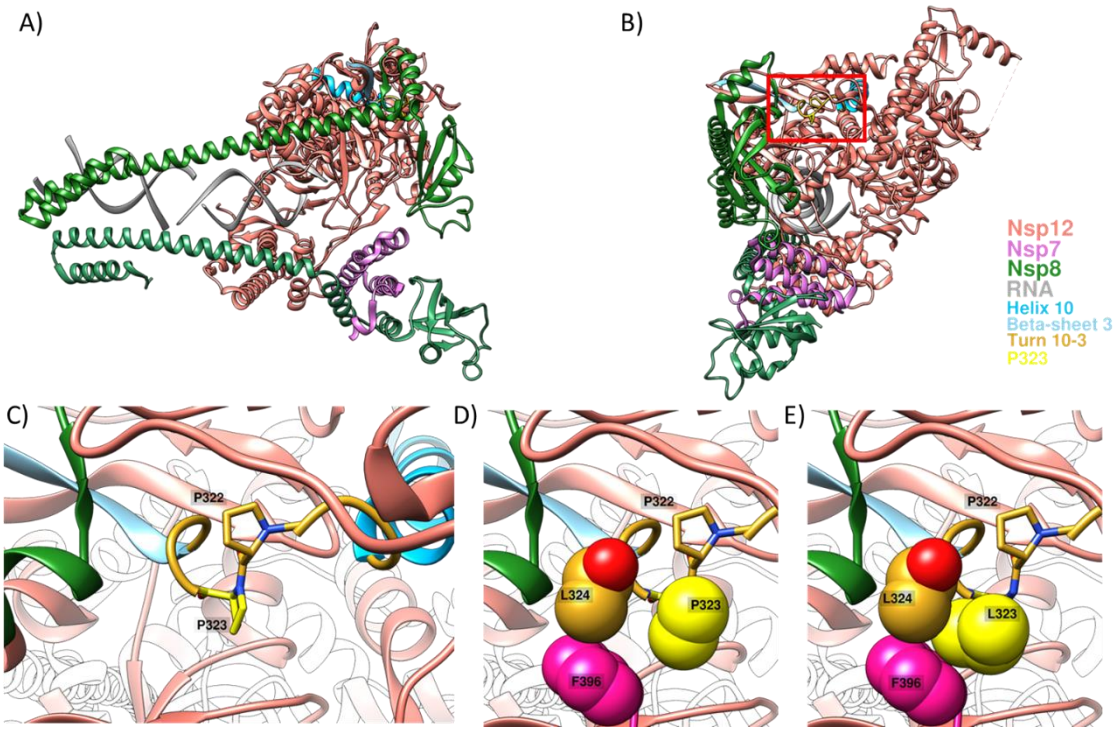

Figure 5. P323L could impact stability of Nsp12 without disturbing its overall structure. A) Structure of RNA-dependent RNA polymerase complex (PDB ID: 6YYT). Chains (Nsp12, Nsp7, Nsp8, RNA) are distinguished by colors. Helix 10, Beta-sheet 3, Turn 10-3 and P323 also are differentially colored. B) Structure in A rotated 90 degrees. C) Zoom of the red box in B showed P322 and P323 in the center of Turn 10-3. D) Turn 10-3 with side chains of P323, L324 and F396 in sphere representation to highlight the distance between side chains of P323 and L324. E) P323 in D was computationally replaced by L323. Now, distances between methyl group of leucine are shorter with L323.

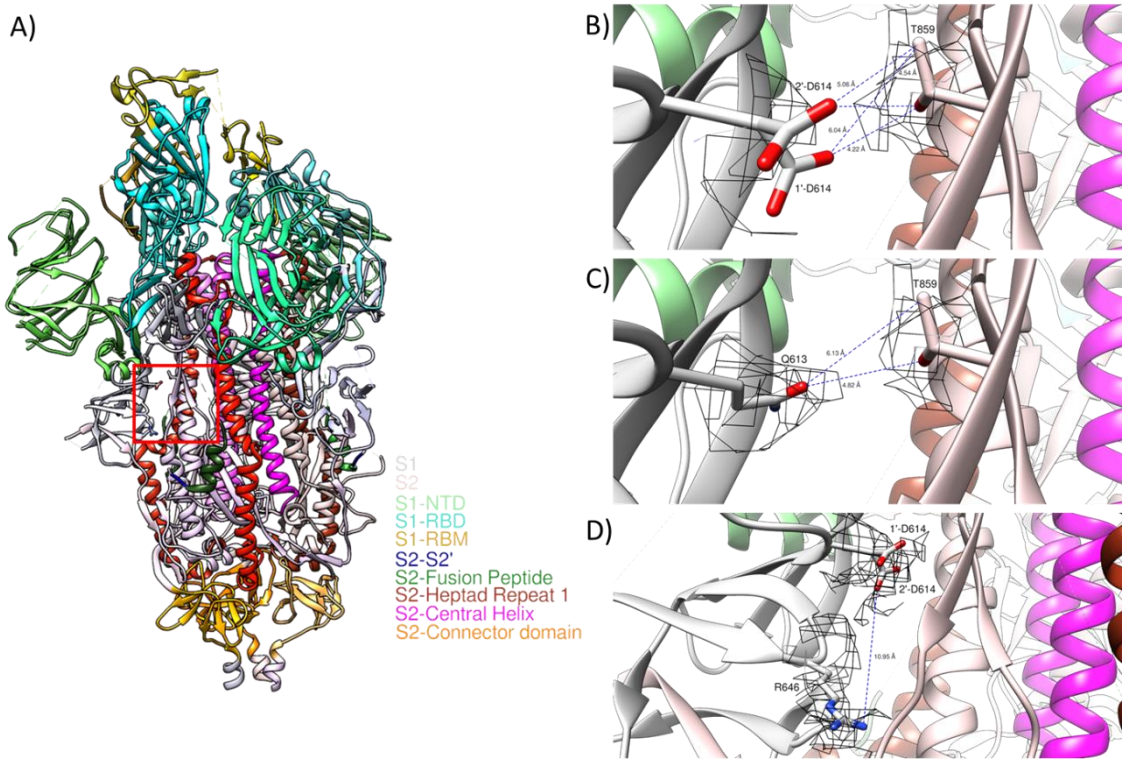

Figure 6. Structural hypotheses about D614G mutation in Spike protein. A) Structure of the open state of Spike trimer (PDB ID: 6YVB) colored by domains. B) Distances between side chains of two possible rotamers of D614 (1`-D614 and 2`-D614) and T859. Except for 1`-D614 and carbonyl group of T859, the other distances seems to be large to form a hydrogen bond. C) Distances between side chains Q613 and T859. These distances are also large to form hydrogen bonds. D) R646 point to the opposite side of D614 showing that there is no salt bridge. B,C and D shows electron density maps of the side chains of the labeled residues.

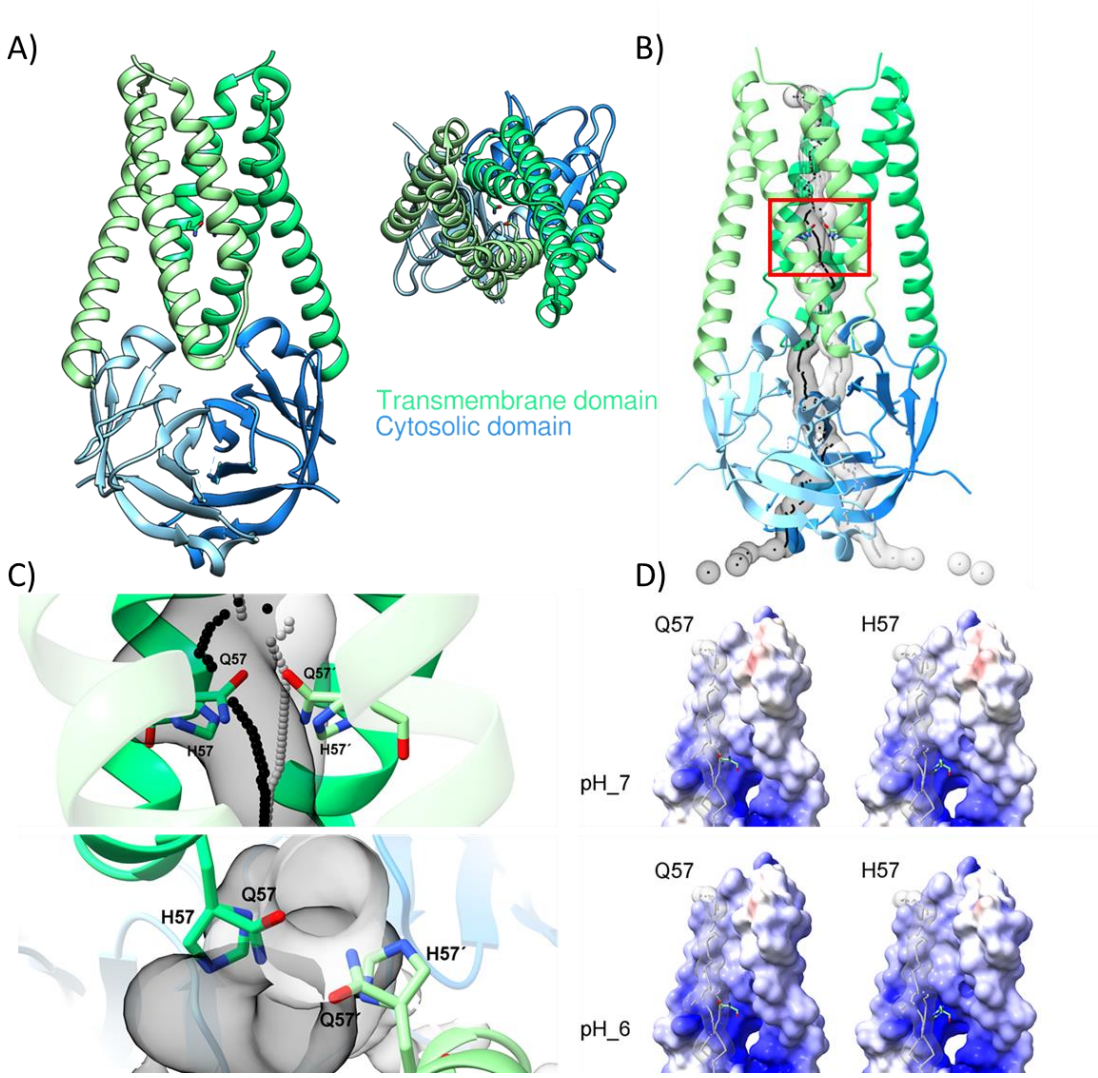

Figure 7. Orf3a Q57H apparently does not modify pore constriction distances but electrostatics distribution. A) Structure of the Orf3a dimer (PDB ID: 6XDC) colored by domains. Right of A shows the same structure but in an upper view. B) Orf3a showing the central pore, in red box the section corresponding to the fifth pore constriction. C) zoom of the red box in B, above we showed Q and H variants superpossed. Below we show a transversal cut of the pore near to the fifth. Pore radius in two variants are similar. D) Electrostatic surface maps of Q57 and H57 variants in two different pHs (7 and 6). Residues Q57 and H57 are shown in stick representations to point the fifth constriction. We show a slighlty more positive region at the height of the fifth constriction.